Applied Catalysis B: Environment and Energy 346 (2024) 123747

Contents lists available at ScienceDirect

Applied Catalysis B: Environment and Energy

journal homepage: www.elsevier.com/locate/apcatb

Mesoporous zeolite ZSM-5 confined Cu nanoclusters for efficient selective catalytic reduction of NO_x by NH_3

Sun Yuanyuan [a], Zhanyu Li [a], Xiaoxia Zhou [b,*], Guohui Li [c], Min Tan [a], Shuang Ao [a], Wei Sun [a], Hangrong Chen [b,*]

[a] Hainan Engineering Research Center of Tropical Ocean Advanced Optoelectronic Functional Materials, Key Laboratory of Laser Technology and Optoelectronic Functional Materials of Hainan Province, Key Laboratory of Functional Materials and Photoelectrochemistry of Haikou, School of Chemistry and Chemical Engineering, Hainan Normal University, Haikou 571158, China

[b] State Key Laboratory of High Performance Ceramics and Superfine Microstructures, Shanghai Institute of Ceramics, Chinese Academy of Sciences, 1295 Dingxi Road, Shanghai 200050, China

[c] School of Science, Qiongtai Normal University, 571127 Haikou, China

ARTICLE INFO

Keywords:
Zeolite ZSM-5
Confinement
Cu^+/Cu^{2+}
NH_3-SCR
in-situ FTIR

ABSTRACT

Cu-based catalysts have been widely used in ammonia-selective catalytic reduction (NH_3-SCR) of NO_x for their excellent low temperature denitration performance. However, the aggregation of Cu species has been a troubling problem in catalyst design. Herein, spherical zeolite ZSM-5 confined Cu nanoclusters Cu@ZSM-5 has been successfully constructed *via in-situ* self-assembly process. It exhibits high specific surface area (373 m^2g^{-1}), higher concentration of Cu^+, rich oxygen vacancies and more acid sites compared with Cu/ZSM-5. The results indicate that strong acid sites of carrier could improve high-temperature catalytic activity, and Cu species as active sites could significantly improve both the low-temperature and high-temperature catalytic reduction activity of NO_x, especially, its performance maintained unchanged after coating on honeycomb ceramics. Thanks to strong surface acidity sites and the confinement effect, the Cu@ZSM-5 exhibited super activity, high N_2 selectivity, wide operating temperature window and strong water resistance.

1. Introduction

Nitrogen oxides (NO_x) is one of the most serious pollutants in the air, which can cause acid rain, photochemical smog and a series of environmental problems [1]. Currently, the most effective and widely used technology for NO_x elimination is ammonia selective catalytic reduction (NH_3-SCR) [2–4]. Therefore, developing denitration catalysts with high activity, excellent selectivity, and strong water resistance is vital.

Among various reported catalysts, Cu-based zeolite is considered as an ideal catalyst for NH_3-SCR reaction due to its good redox capacity, suitable acidity intensity and high hydrothermal stability [5–7]. For example, He *et al.* studied the catalyst Cu-SSZ-39 prepared using four precursors, and found that Cu-SSZ-39 prepared using ZSM-5 as precursor exhibited the best low-temperature NH_3-SCR activity and hydrothermal stability [8]. Besides, conventional zeolite supported metal nanoparticles catalysts is easily deactivated in catalytic reactions, because metal nanoparticles will migrate and aggregate at high temperatures due to Ostwald ripening [9–11]. In recent years, researchers have developed a new method of encapsulating metal nanoparticles into zeolites, which can greatly hinder the aggregation of metal nanoparticles and thus improve the catalytic activity [12–14]. For example, Wu et al. prepared a high-silica Cu/ZSM-5 with confinement encapsulated Cu species for the catalytic process of NH_3-SCR, exhibiting excellent catalytic performance and structural stability [15]. Peng *et al.* designed $MnCeO_x$ @ZSM-5 for selective catalytic reduction of NO_x with NH_3, and found that the enhanced performances could be attributed to the confinement and the acid-redox synergy strategy [12]. However, the micropore size of conventional zeolites is less than 2 nm, which not only greatly limit the diffusion and mass transfer of reactants and products, but also affect the availability of metal active sites [9,16–18]. Therefore, creating mesoporous channels in conventional zeolite is believed to be an efficient method to improve mass transfer efficiency and the accessibility of active sites. Compared with conventional micropore zeolites, mesoporous zeolites show significantly advantages in catalysis, such as achieving metal species with high dispersity, accelerating the diffusion and mass transfer, improving coking resistance and *et al.* [19–21].

* Corresponding authors.
E-mail addresses: zhouxiaoxia@mail.sic.ac.cn (X. Zhou), hrchen@mail.sic.ac.cn (H. Chen).

https://doi.org/10.1016/j.apcatb.2024.123747
Received 11 November 2023; Received in revised form 7 January 2024; Accepted 15 January 2024
Available online 17 January 2024

Therefore, it is attractive to fabricate a novel Cu-encapsulated mesoporous zeolite with desired catalytic properties in the application of the NH_3-SCR process. For example, Liu *et al.* reported Fe species loaded hierarchical ZSM-5 zeolites with nanosheet-assembled structure, which showed super NH_3-SCR activity with higher NO_x conversion (> 90%) over a broad temperature window (250–425 °C) [22]. They also designed a hierarchical porous Cu-ZSM-5 zeolite by an ion-exchanged method, which showed improved catalytic performance in NH_3-SCR reaction comparing to conventional zeolite [23]. However, their reported Cu-based zeolites were basically obtained by an ion-exchange method, and the creature of hierarchical zeolite ZSM-5 often requires high cost of organic templates, limiting its popularity. [24,25]. Our previous studies found that the introduction of sodium carbonate into the precursor solution can not only induce nanocrystalline aggregates, but also form abundant hierarchical pores between nanocrystalline aggregates [26]. More importantly, this synthesis method does not require additional organic templates and is environmentally friendly, which provides a good reference for the synthesis of mesoporous zeolite.

It is reported that the Brønsted acid sites can accelerate the adsorption of NH_3 at higher temperatures, while Cu active sites are responsible for the NH_3 adsorption at lower temperature [22,27,28]. Therefore, zeolite ZSM-5 with rich Brønsted acid sites and desirable active sites can be used as an ideal carrier material for the NH_3-SCR reaction. Encapsulating abundant Cu species into mesoporous zeolite ZSM-5 is expected to improve NH_3-SCR activity and broaden the reaction window by the cooperation between mesoporous zeolite ZSM-5 and Cu active sites. Especially, the confinement effect by zeolites is more significant due to its well-ordered and rigid structure compared with other catalysis systems [22,29]. The spatial and electronic properties of active sites confined in zeolites may induce the activation of reactant. More importantly, the interaction between subnanometer metal clusters and zeolite skeleton atoms can regulate their geometric and electronic structures, further improving its catalytic performance and product selectivity [29,30]. Until now, new high-stable mesoporous zeolite-confined metal nanoparticles (NPs) for high-efficient NH_3-SCR reaction should be rationally designed, and the multiple effect from zeolite confinement requires carefully assessment.

Based on above results, a simple *in-situ* synthesis strategy was proposed to design Cu nanoclusters-encapsulated mesoporous zeolite ZSM-5 (Cu@ZSM-5) with rich three-dimensional hierarchically pores structure. The aim is to induce the synergistic interaction between Cu nanoclusters and zeolite skeleton with intrinsic acidic site by the confinement effect, further improving the NH_3-SCR of NO_x performance. Such designed catalyst showed excellent NO_x conversion (close to 100%) with higher N_2 selectivity at 200–475 °C. Besides, mesoporous zeolite ZSM-5 supported Cu nanoparticles Cu/ZSM-5 has been prepared for comparison. The zeolite confinement effect in the NH_3-SCR has been deeply studied, including Cu valence state, oxygen vacancies, surface acidity, adsorption and activation capacity of reactants and stability as well as durability. Interestingly, Cu@ZSM-5 exhibited remarkable water tolerance ability compared with Cu/ZSM-5, indicating that zeolite confined catalyst could effectively inhibit the competitive adsorption between NO_x/NH_3 and H_2O. This work provide a fundamental understanding of zeolite confinement effect in NH_3-SCR, providing reference for the rational design of Cu-based denitration catalysts.

2. Experimental section

2.1. The preparation of the samples

2.1.1. Synthesis of mesoporous zeolite ZSM-5 (ZSM-5)

The synthesis process of hierarchical porous zeolite ZSM-5 is similar to our previous work [26]. In a typical experiment, 4.2 g of Tetrapropylammonium hydroxide (TPAOH, 40% in water, J&K) was added into 10 g distilled water solution including 0.12 g Na_2CO_3 under stirring conditions. Subsequently, 50 mmol H_2SiO_3 were dissolved into the above solution and stirred at 40 °C for 4 h. Next, a sodium hydroxide solution including 1 mmol $NaAlO_2$ and 3 g H_2O was added to the mixture and aged at 40 °C for 4 h. Finally, the mixture was placed in a Teflon-lined stainless steel autoclave and treated at 150 °C for 24 h. The resulting product was washed three times with deionized water and then freeze-dried. The final sample was collected after calcined at 550 °C for 6 h and denoted as ZSM-5.

2.1.2. Synthesis of mesoporous zeolite ZSM-5 supported Cu (Cu/ZSM-5)

The mesoporous zeolite ZSM-5 supported Cu was prepared by a simple impregnation method. The obtained powder zeolite ZSM-5 was added into a solution of the desired amount of $Cu(CH_3COO)_2{\cdot}4\ H_2O$, with a zeolite/liquid ratio of 1 $g{\cdot}L^{-1}$, and the resulting solution was stirred for 6 h at 40 °C. Finally, the powder was dried and calcined at 550 °C for 4 h, and the obtained sample was denoted as Cu/ZSM-5.

2.1.3. Synthesis of Cu-encapsulating mesoporous zeolite ZSM-5 (Cu@ZSM-5)

A series of Cu-encapsulated mesoporous zeolite ZSM-5 was prepared following the process of mesoporous zeolite ZSM-5, except that Cu $(CH_3COO)_2{\cdot}4\ H_2O$ solution was added to the synthetic mixture. Herein, the Cu/Si molar ratio was adjusted as 0.01, 0.02 and 0.04, and was labeled as Cu@ZSM-5 (n) (n = 1, 2, 3), respectively.

2.1.4. Synthesis of monolithic catalyst

20 g powder was added into 60 g H_2O including 10 g aluminium sol (pH = 5), then the mixed solution was ball-milled for 12 h to obtain slurry. Next, the slurry was coated on the cordierite honeycomb ceramics (2.4 mm × 2.4 mm×7.5 mm) of 400 mesh, and the final monolithic catalyst was dried and calcined at 450 °C.

2.2. Characterization

Powder X-ray diffraction (XRD) measurement for the samples was performed on a Phillips X-ray diffractometer using Cu Kα radiation in the 2θ of 5 to 60°. Scanning electron microscopy (SEM) images were acquired on Field Emission Scanning Electron Microscope (FEI, 125 Magellan 400) using an HAADF detector to investigate the morphology and element distribution of the samples. Transmission electron microscopy (TEM, JEOL-2010 F) and high-resolution TEM (HRTEM) were used to study the microstructure of samples. X-ray photoelectron spectroscopy (XPS, Thermo) was adopted to investigate the valence state of the elements of the samples. The surface area and pore size distribution curves of the samples were determined by N_2 sorption and desorption at − 196 °C. The temperature programmed desorption of ammonia (NH_3-TPD) and the temperature-programed reduction with hydrogen (H_2-TPR) were tested on Micromeritics Chemisorb 2750 instrument. X-ray absorption spectroscopy (XAS) are carried out a synchrotron radiation photoemission spectroscopy from Thermo Fisher Scientific [ESCA-lab250], and the incident X-ray source is 650 eV with a base pressure of 5×10^{-10} Torr. The content of element was tested on inductively coupled plasma optical emission spectrometer (ICP-OES).

2.3. Catalytic tests

The NH_3-SCR activity of powder samples was evaluated in a fixed-bed quartz reactor, and the 100 mg catalysts were filled into the reaction tubes before reaction. The composition of the feed gas was 500 ppm NO, 600 ppm NH_3, 8 vol% H_2O, 8 vol% O_2, and balance N_2. The total flow rate was controlled at 300 $mL{\cdot}min^{-1}$, and the corresponding gas hourly space velocity (GHSV) was about 40000 h^{-1}. The reaction was carried out from 100 to 600 °C, and each measuring point of the powder catalyst is insulated for 15 min in order to obtain stable sampling data, and then the product gas was analyzed by a Thermo NO_x analyzer. Besides, the NH_3-SCR activity of monolithic catalyst was evaluated by a MSK FTIR detector, and the composition of feed gas and GHSV are the

same as that of powder catalyst. The conversion of NO_x and NH_3 equation is:

$$NO_x \quad conversion\% = \frac{(NO_x)in - (NO_x)out}{(NO_x)in} * 100\% \tag{1}$$

$$NH_3 \quad conversion\% = \frac{(NH_3)in - (NH_3)out}{(NH_3)in} * 100\% \tag{2}$$

While, N_2 selectivity was calculated from

$$N_2 \quad selectivity\% = [1 - \frac{2(N_2O)out}{(NO_x)in + (NH_3)in \quad -(NO_x)out - (NH_3)out}] * 100\% \tag{3}$$

The NH_3-SCR kinetic parameter was evaluated based on the NO_x conversion below 15% to minimize the influence of mass and heat transfer, and was calculated according to the following formula:

$$k = -\frac{F_{NOx}}{W} \times \ln(1 - x) \tag{4}$$

$$\ln k = -\frac{E_a}{RT} + C \tag{5}$$

Herein, k is the reaction rate ($cm^3\ g^{-1}\ s^{-1}$); F_{NOx} is the NO_x flow rate ($cm^3\ s^{-1}$); w is the mass of the catalyst (g) and x is the conversion of NO_x; T and R are reaction temperature (K) and ideal gas constant, respectively, and C is generally regarded as a constant. E_a is the apparent activation energy (kJ mol^{-1}) which was calculated from the slope of the Arrhenius plot.

3. Results and discussion

3.1. The properties of powder samples

The synthesis schematic of Cu nanoclusters encapsulated zeolite ZSM-5 with mesoporous structure is shown in Fig. 1a. The Cu species were assembled into zeolite framework and mesoporous channel under the action of the structural directing agent TPAOH and carbonate. Among, the carbonate plays an important role in the introduction of mesopore, similar to our previous report [26]. The XRD patterns in Fig. S1 shows that the diffraction peaks of the samples Cu@ZSM-5, ZSM-5 and Cu/ZSM-5 are similar to those of pure-phase MFI zeolite ZSM-5 (PDF:# 03–0359), and no obvious peaks corresponding to Cu species can be observed. This result indicates that Cu species could enter into zeolite framework in the form of ions or be encapsulated into mesoporous channels in the form of Cu nanoclusters. Additionally, among these three catalysts, Cu@ZSM-5 and Cu/ZSM-5 maintain a relative weak diffraction peak compared with that of ZSM-5, indicating that there are slight collapse of zeolite framework with the introduction of Cu.

Pure zeolite ZSM-5 exhibits regular quasi-spherical morphology, and the contrast between light and dark suggests the presence of mesopore. Additionally, the EDX spectrum and the element mapping images also confirm the uniform dispersion of Si, Al and O in the zeolite ZSM-5 (Fig. S2). After confining Cu species in the zeolite ZSM-5, the obtained catalyst Cu@ZSM-5 still presents regular quasi-spherical morphology with the size of 300–500 nm according to the SEM and TEM images (Fig. 1b-c). Additionally, the interplanar distance of Cu@ZSM-5 is around 1.11 nm, corresponding to the typical (101) plane of zeolite ZSM-5 (Fig. 1d). From the element mapping images (Fig. 1f-i) and EDX spectrum of Fig. 1d (Fig. S3), it is noted that the Si, Al, O and Cu species are uniformly distributed on the sample Cu@ZSM-5, which is

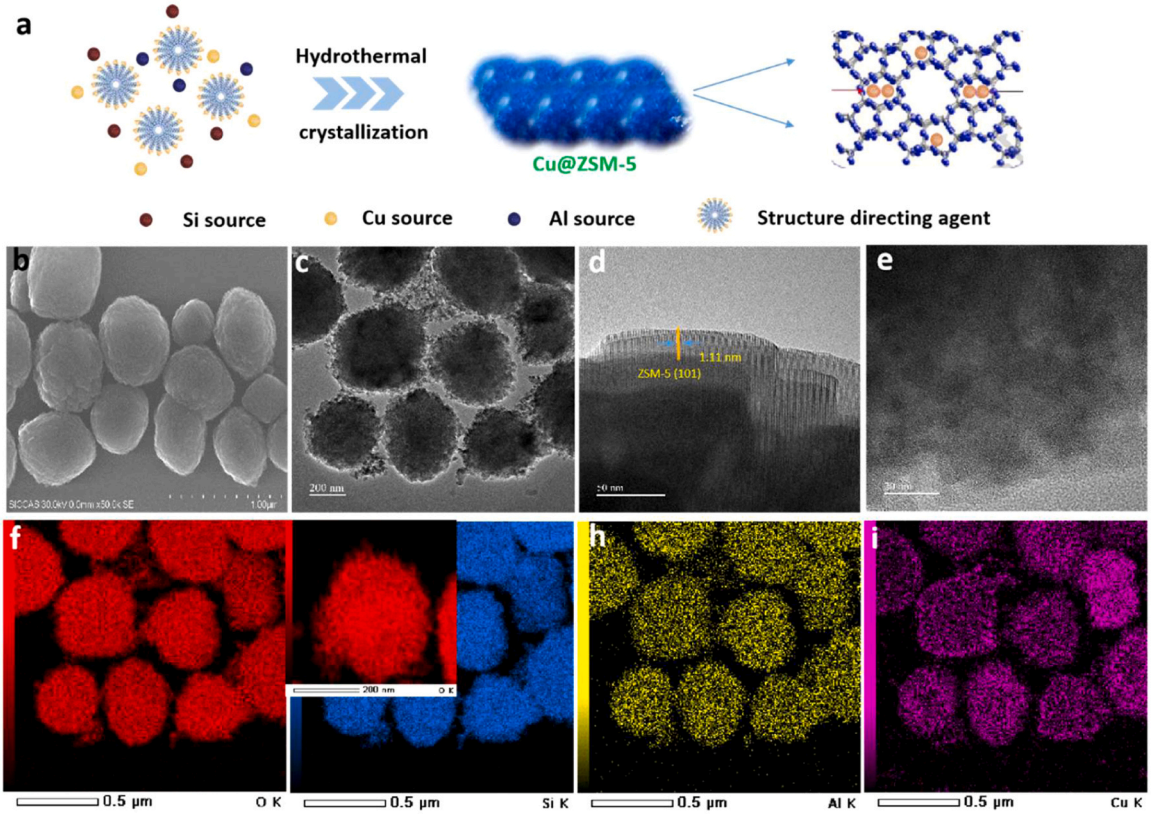

Fig. 1. a) The synthetic schematic of zeolite ZSM-5 confined Cu nanoclusters catalyst Cu@ZSM-5, b) SEM, c-e) TEM and HRTEM images, f-i) element mapping images of the sample Cu@ZSM-5.

conductive to enhance the interaction between Cu species and zeolite matrix. In contrast, the reference sample Cu/ZSM-5 obtained by the post impregnation still shows regular morphology (Fig. S4), but the Cu species mainly concentrate on the surface of zeolite (Fig. S4g), which is different from that of Cu@ZSM-5. Clearly, the prepared catalyst Cu@ZSM-5 has higher Cu dispersion than the Cu/ZSM-5, which is beneficial for exposing more active sites to promote the adsorption and NO_x conversion. Furthermore, spherical aberration corrected high-resolution TEM bright field images of the sample Cu@ZSM-5 have been provided to observe Cu species, As shown in Fig. 2a-b, the uniformly dispersed bright spots verify the existence of well-dispersion Cu nanoparticles and nanoclusters smaller than 5 nm throughout the zeolite. Besides, the corresponding EDS spectrum of Fig. 2b also proves the existence of Cu species, as shown in Fig. 2c. Notably, the size of Cu nanoclusters is much larger than that in the zeolite ZSM-5 micropore (*ca.* 0.55 nm), thus Cu nanoclusters are mainly confined in the mesoporous channels [31].

N_2 adsorption-desorption isotherms and the corresponding pore size curves of the samples Cu@ZSM-5, Cu/ZSM-5 and ZSM-5 are shown in the Fig. 3, and the pore structural parameters of three samples are listed in Table S1. The typical isotherms of type-I and type-IV indicate the presence of the micropore and mesopore, which is helpful to provide rich active sites for the adsorption of the reactant. The pure ZSM-5 shows high BET surface area (431 m^2g^{-1}) and larger pore volume (0.47 cm^3g^{-1}) with the average pore size of 4.3 nm. Compared with pure ZSM-5, Cu@ZSM-5 shows a relatively lower BET surface area (373 m^2g^{-1}) and smaller pore volume (0.32 cm^3g^{-1}) with the average pore size of 3.5 nm, which are resulted from the Cu nanoclusters confined into the mesoporous channels. Similarly, the reference Cu/ZSM-5 also shows lower BET surface area and smaller pore volume.

H_2-TPR profiles of the catalysts Cu@ZSM-5, Cu/ZSM-5 and ZSM-5 are conducted to explore the distribution of Cu sites, as presented in Fig. 4a. The peak around 400 ℃ is attributed to the reduction of Cu^{2+} species to Cu^+ [32,33], while the peak at 600–700 ℃ is assigned to the reduction of Cu^+ to Cu [8]. It is evident that the Cu^{2+} species of Cu@ZSM-5 can be easily reduced to Cu^+ species and lead to strong redox peak around 400 ℃, indicating that the confinement effect of mesoporous zeolite can regulate the distribution of Cu species.

NH_3-TPD experiments and Pyridine adsorbed FT-IR spectra are carried out to investigate the amount and intensity of acid sites of the samples Cu@ZSM-5, Cu/ZSM-5 and ZSM-5. NH_3-TPD peaks (Fig. 4b) at lower temperatures of 100–300 ℃ are assigned to weak acid, while the peaks at higher temperatures of 300–550 ℃ are attributed to strong acid sites [8,27]. Clearly, the Cu@ZSM-5 and Cu/ZSM-5 shows obviously decreased amounts of weak acid and strong acid after introduction of Cu species, which is consistent with previous reports [34]. Moreover, the FT-IR spectra of pyridine adsorbed have also been carried out to evaluate the acidity of the samples, as shown in Fig. 4c-d. The bands at 1540 cm^{-1} and 1450 cm^{-1} are ascribed to pyridine chemisorbed on the Brønsted acid sites and Lewis acid sites, respectively [34]. In addition, the peaks at 1490 cm^{-1} are associated with the pyridine chemisorbed on both Lewis and Brønsted acid sites. The amounts of weak and strong acid sites are calculated based on the pyridine adsorption at 200 ℃ and 400 ℃, respectively, and the results are listed in Table 1. Compared with that of ZSM-5, the amounts of Lewis acid and Brønsted acid of the samples Cu@ZSM-5 and Cu/ZSM-5 are decreased due to the dealumination of the ZSM-5 zeolite and the formation of highly agglomerated oxide species during Cu modification (Fig. 2a-b), which is also consistent with the NH_3-TPD results. Notably, it is found that the sample Cu@ZSM-5 shows higher Lewis acid and Brønsted acid sites than the Cu/ZSM-5, and the concentrations of total acid sites of the samples Cu@ZSM-5 and Cu/ZSM-5 are calculated to be 193.9 and 119.7 μmol g^{-1}, respectively. Besides, the concentrations of metal atoms (Al and Cu) of the samples Cu@ZSM-5 and Cu/ZSM-5 is about 920 μmol g^{-1}, and the ratio of total acid site concentrations to the number of Al and Cu atoms in the samples Cu@ZSM-5 and Cu/ZSM-5 are about 0.211 and 0.130, respectively, indicating that the obtained Cu@ZSM-5 shows greatly improved Cu species dispersion by *in-situ* self-assembly process. Thanks to the mesoporous zeolite-confined Cu nanoclusters, the catalyst Cu@ZSM-5 exhibits more acid sites than that of Cu/ZSM-5, which is beneficial for improving NH_3-SCR performance.

The valence states of elements on the catalyst surface are analyzed with XPS, as shown in Fig. 5. The survey spectra of Cu@ZSM-5 and Cu/ZSM-5 indicate the co-existence of Si, Al, O and Cu. The Si 2p peak of Cu@ZSM-5, Cu/ZSM-5 and ZSM-5 (Fig. 5b) located at 103.6–104.2 eV is characteristic for the Si-O (SiO_2) bond [35]. The Si 2p peak shifts toward higher binding energy with the introduction of Cu species, indicating that there exists interaction between Cu and zeolite framework. Compared with Cu/ZSM-5, Al 2p peak of Cu@ZSM-5 is significantly broadened (Fig. 5c). This implies that the charge transfer from Al to Cu, resulting in the reduction of the Cu^{2+} and the oxidation of Al atom[36]. High-resolution O 1 s peaks are shown in Fig. 5d, and three fitting peaks are successively attributed to the surface adsorbed oxygen (O_c), O-H species and O-M (M: Al or Cu), respectively [37,38]. Compared with Cu/ZSM-5 and ZSM-5, Cu@ZSM-5 has the highest O_c content (52.4%), which is conducive to the adsorption and activation of reactants. For Cu 2p XPS spectra of Cu/ZSM-5 and Cu@ZSM-5, these peaks located at 933.8–933.9 eV are attributed to Cu^+ species, while the peaks centered at 955.7–955.8 eV and 935.8–936 eV are assigned to Cu^{2+} species. Meanwhile, the shake-up satellite peaks also further prove the presence of Cu^{2+} species [33,39]. Additionally, the sample Cu@ZSM-5 shows more Cu^+(47.2%) than the Cu/ZSM-5 sample (40.8%), combined with the broad Al 2p peak of Cu@ZSM-5. It can be included that Cu species can be strongly bound to Al atoms and cause charge transfer from Al to Cu due to the confinement effect, which can result in the reduction of the Cu^{2+} to Cu^+, further suggesting the strong interaction between the Cu species and the zeolite matrix [39].

X-ray absorption spectroscopy (XAS) has also been adopted to further analyze the chemical state and electron structure of the samples Cu@ZSM-5 and Cu/ZSM-5, as shown in Fig. 6. The Cu K-edge XANES spectra of Cu@ZSM-5, Cu/ZSM-5 and the references CuO, Cu_2O and Cu foil are shown in Fig. 6a. It is found that the absorption edge of

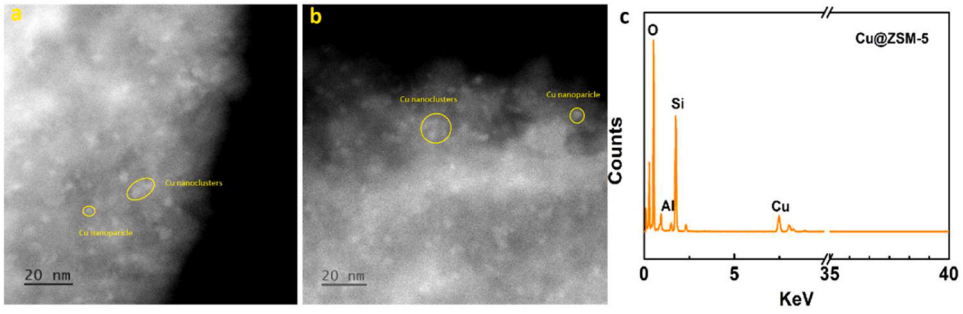

Fig. 2. a-b) Spherical aberration corrected high-resolution TEM bright field images and c) the corresponding EDS spectra of Fig. 2b for the sample Cu@ZSM-5.

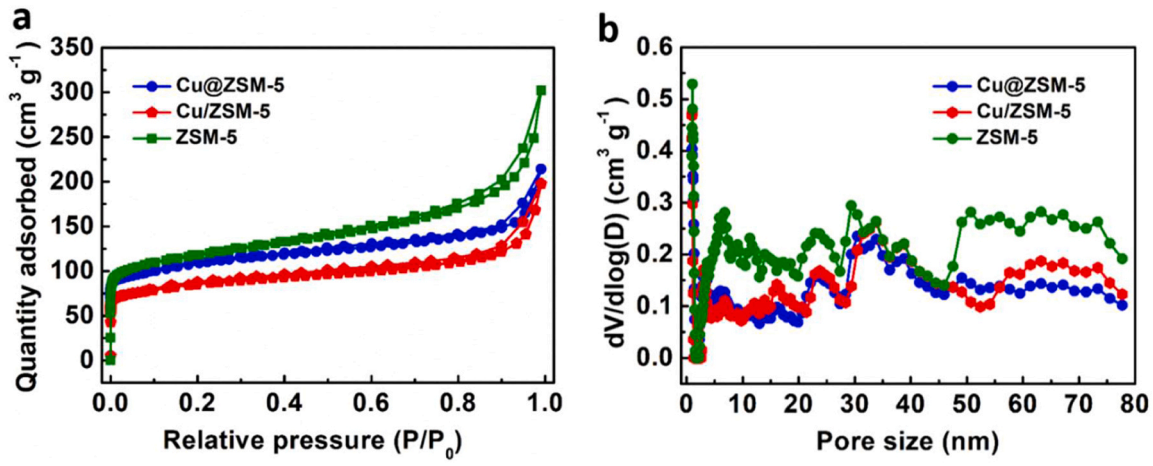

Fig. 3. a) N_2 adsorption and desorption curves and b) the corresponding pore size distribution curves of the samples Cu@ZSM-5, Cu/ZSM-5 and ZSM-5.

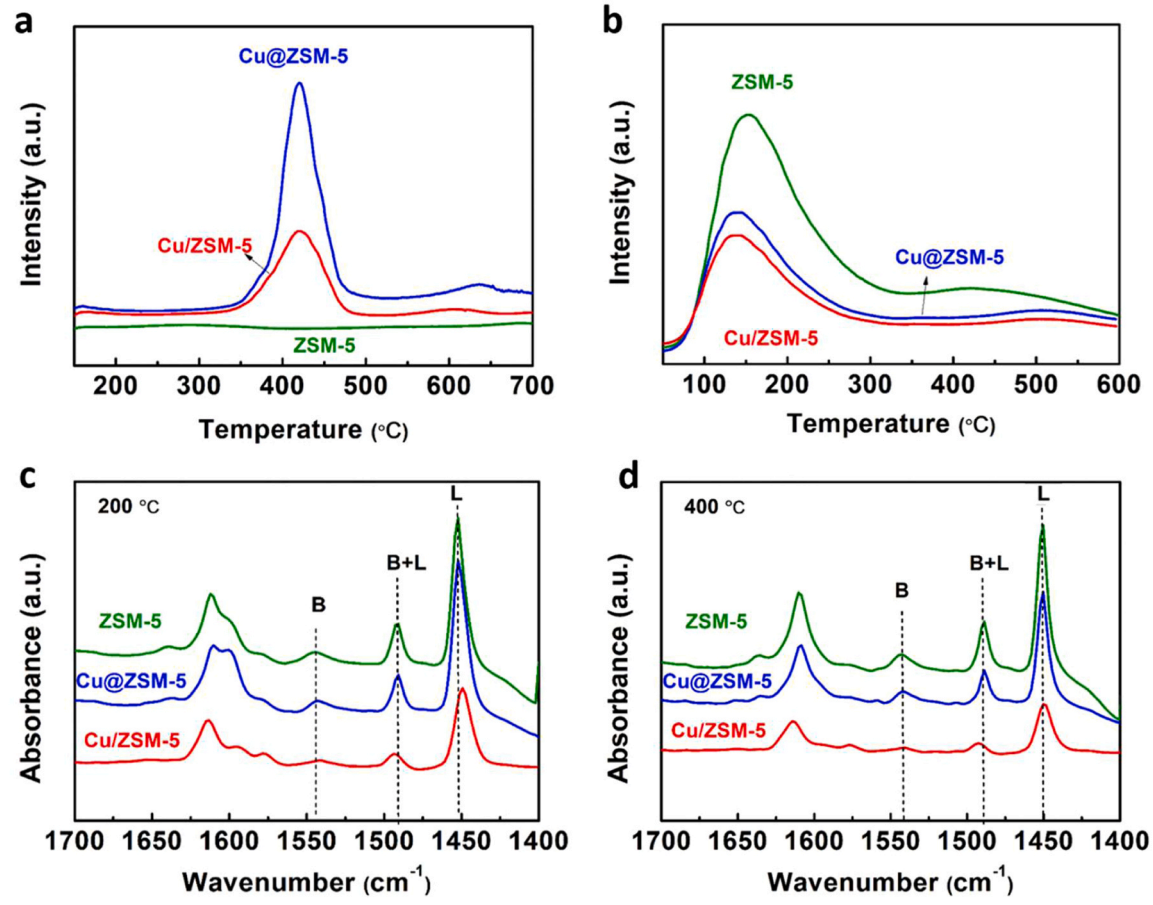

Fig. 4. a) H_2 temperature programmed reduction (H_2-TPR), b) NH_3 temperature programmed desorption (NH_3-TPD) profiles, Pyridine adsorbed FT-IR spectra at 200 ℃ (c) and 400 ℃ (d) for the samples Cu@ZSM-5, Cu/ZSM-5 and ZSM-5.

Cu@ZSM-5 and Cu/ZSM-5 between the Cu_2O and CuO, indicating that the oxidation state of Cu is between + 1 and + 2 due to the coexistence of Cu^+ and Cu^{2+}. Besides, there are more low-valence Cu presented in the sample Cu@ZSM-5 compared with Cu/ZSM-5, which is consistence with the XPS results. The Fourier-transformed (FT) K3-weighted EXAFS spectra are shown in Fig. 6b. No peak corresponding to Cu-Cu bond can be observed on the samples Cu@ZSM-5 and Cu/ZSM-5, while the peak assigned to Cu−O can be observed at 1.50 Å, and the coordination number (CN) is 3.31 for the sample Cu@ZSM-5, as shown in Table S2. The atomic configuration of the samples Cu@ZSM-5 and Cu/ZSM-5 is further analyzed by wavelet transform (WT) EXAFS (Fig. 6c). The WT contour plots of Cu@ZSM-5 and Cu/ZSM-5 also display an intensity maximum close to 6.1 Å^{-1} corresponding to the Cu-O coordination. This result indicates that Cu species of the samples Cu@ZSM-5 and Cu/ZSM-5 exist mainly in the form of CuO coordinated by four oxygen atoms. Additionally, the CN of Cu-O on the sample Cu@ZSM-5 is lower than that on the reference CuO (CN = 4) and Cu/ZSM-5 (3.40), which is ascribed to the presence of more coordination-unsaturated Cu-O

Table 1
Concentrations of Lewis acid (1450 cm^{-1}) and Brønsted acid (1540 cm^{-1}) sites of the samples based on the results of Pyridine adsorbed FT-IR spectra.

Samples	Weak acid sites (umol g^{-1})			Strong acid sites (umol g^{-1})			Total acid sites (umol g^{-1})
	B	L	B+L	B	L	B+L	
ZSM-5	20.5	138.2	158.7	15.6	80.2	95.8	354.5
Cu@ZSM-5	16.9	121.4	138.3	10.2	45.4	55.6	193.9
Cu/ZSM-5	7.4	80.3	87.7	2.7	29.3	32.0	119.7

structure due to confinement effect [40].

Fig. 7a displays the NO_x conversion of different samples in the temperature range of 150- 600 ℃. Obviously, the pure zeolite ZSM-5 only showed good catalytic activity at higher temperatures, indicating that a larger number of weak acid sites are difficult to react with NO_x while relatively small amounts of strong acid sites play an important role in NO_x conversion [28]. Thus the catalytic activity of zeolite ZSM-5 is primarily derived from the strong acid sites. After introducing Cu species, the NO_x conversion shows a significant improvement in the wide range of 100–600 °C, indicating that Cu species as active site can significantly improve both the low-temperature and high-temperature catalytic reduction activity of NO_x. Therefore, the excellent activity of the samples Cu/ZSM-5 and Cu@ZSM-5 can be ascribed to the combined effect of acid sites and Cu sites. Especially, zeolite-confined Cu nanoclusters Cu@ZSM-5 achieves above 90% NO_x conversion across a wide temperature range (225–550 °C), and shows up to 98% NO_x conversion at 275–425 °C. Although Cu@ZSM-5 and Cu/ZSM-5 have similar Cu^{2+}/Cu^{+} ratio, the Cu@ZSM-5 has more acid sites (Fig. 4b). Besides, the confined effect of Cu@ZSM-5 is also conductive to the dispersion of Cu species (Fig. 1i and 2a-bg). Therefore, the sample Cu@ZSM-5 shows much superior catalytic activity to that of the Cu/ZSM-5. The above

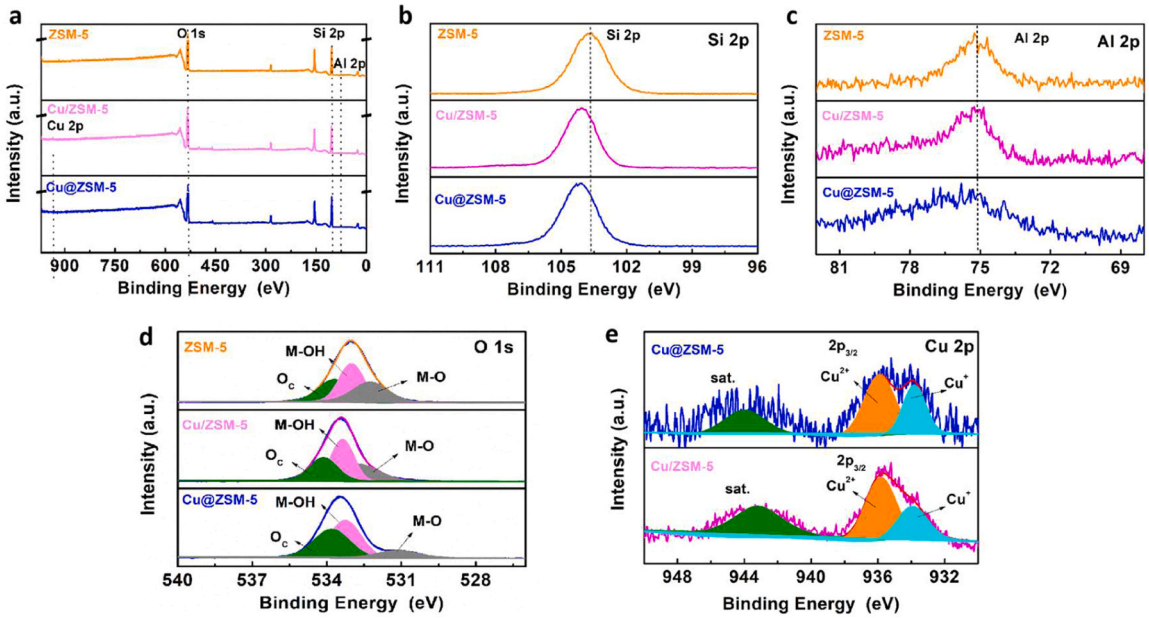

Fig. 5. High-resolution XPS spectra for the samples Cu@ZSM-5, Cu/ZSM-5 and ZSM-5, a) survey, b) Si 2p, c) Al 2p, d) O 1 s and e) Cu 2p.

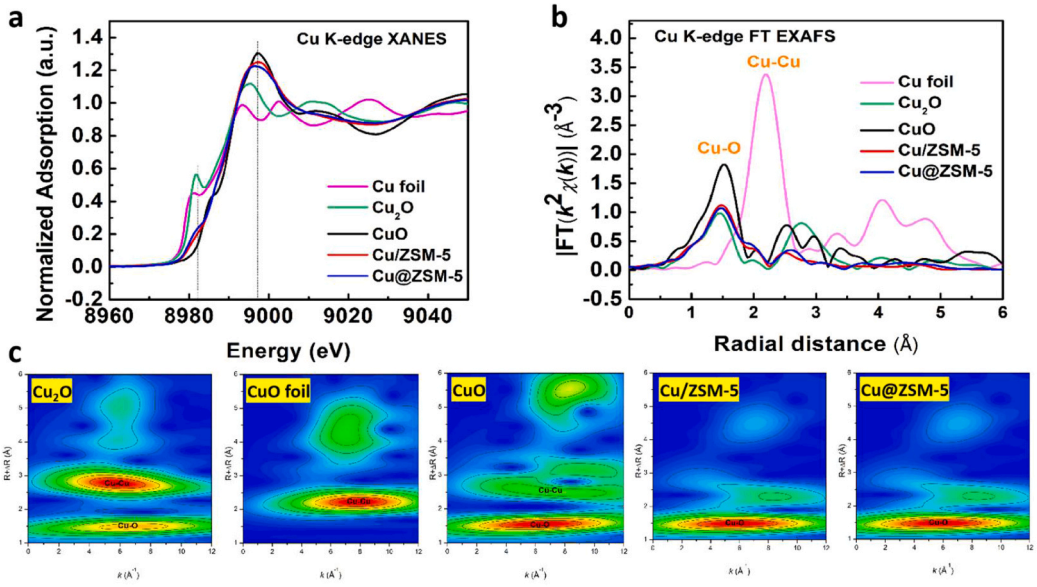

Fig. 6. a) Cu K-edge XANES spectra, b) FT-EXAFS spectra and c) WT-EXAFS of the samples Cu@ZSM-5 and Cu/ZSM-5 with the references from top to bottom.

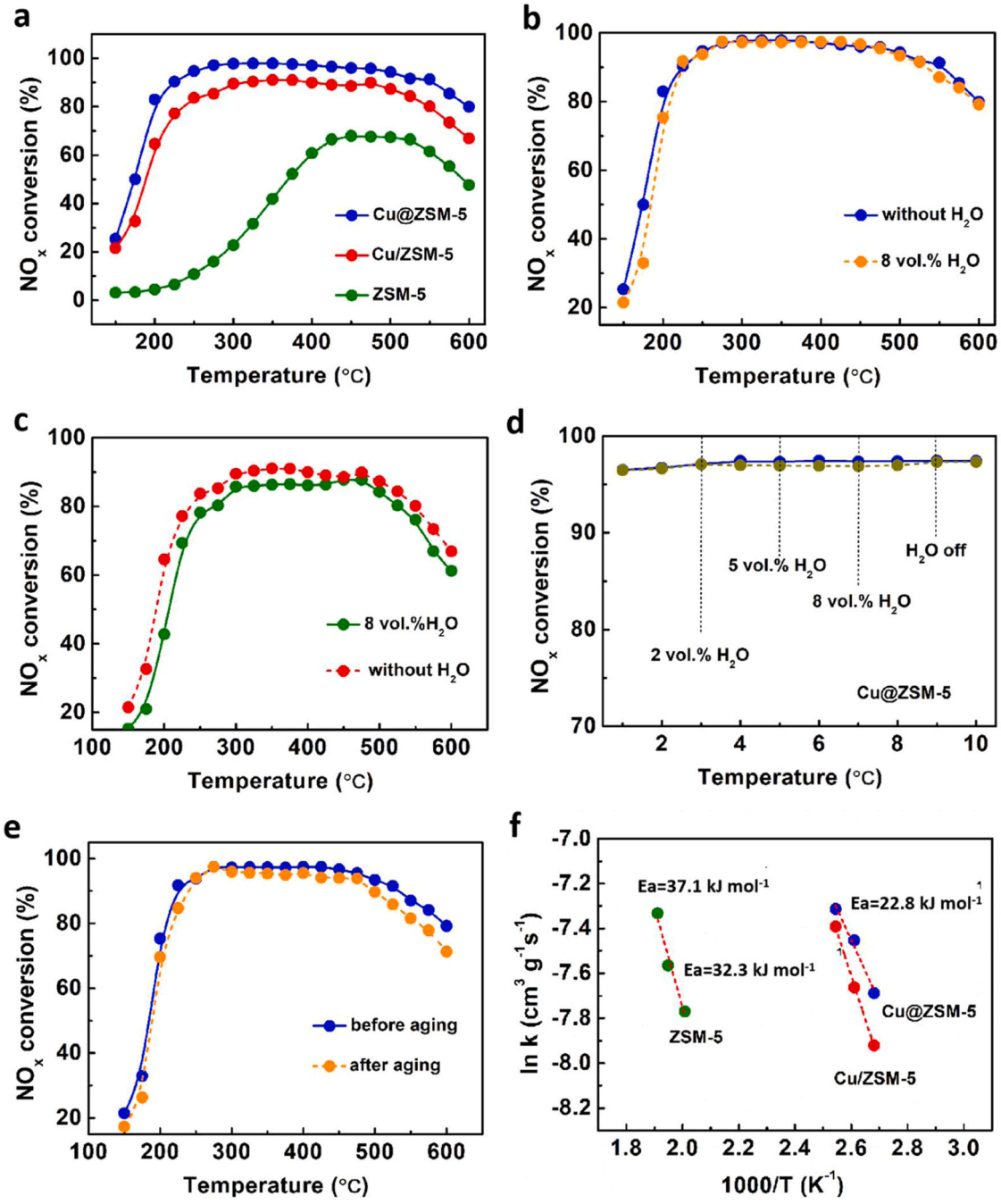

Fig. 7. a) NO_x conversion as a function of temperature of different catalysts Cu@ZSM-5, Cu/ZSM-5 and ZSM-5 under dry reaction atmosphere, b) NO_x conversion of the sample Cu@ZSM-5 in the presence of H_2O, c) NO_x conversion of the sample Cu/ZSM-5 in the presence of H_2O, d) H_2O resistance tests of catalyst Cu@ZSM-5 at 350 °C, e) NO_x conversion of the sample Cu@ZSM-5 before and after aging treatment in the presence of H_2O. (Aging treatment condition: hydrothermally treated for 4 h at 850 °C) and f) Arrhenius equation plots. Reaction conditions: $[NO_x] = 500$ ppm, $[NH_3] = 600$ ppm, $[O_2] = 8$ vol%, $[H_2O] = 8$ vol%, N_2 balanced, and GHSV = 40000 h^{-1}.

results indicate that high catalytic performance of Cu@ZSM-5 are mainly ascribed to the combined effect of the acid sites, the Cu^{2+}/Cu^{+} pairs and the porous confinement effect. Additionally, it is found that the NO_x conversion of the sample Cu@ZSM-5 is positive correlation with Cu content (Fig. S5), However, the Cu@ZSM-5 catalyst with higher Cu content (5.79%) presents lower NO_x conversion due to the aggregation of high-content Cu nanoclusters. Thus, the catalyst Cu@ZSM-5 with suitable Cu content (3.68%) are adopted to further explore the catalytic activity and kinetics. Furthermore, the water resistance of the samples Cu@ZSM-5 and Cu/ZSM-5 has been investigated, and it is encouraging that the sample Cu@ZSM-5 also maintains much superior NO_x reduction performance to that of the Cu/ZSM-5 in the presence 8 vol% H_2O, as shown in Fig. 7b-c. Besides, it is found that the NO_x reduction activity is almost unchanged with the addition of different H_2O content on the sample Cu@ZSM-5 (Fig. 7d), indicating that zeolite-confined catalyst could effectively inhibit competitive adsorption of H_2O. Furthermore, the catalytic activity is almost completely restored when H_2O is turned off, suggesting that the deactivation is reversible, most likely from adsorption of H_2O [41]. Besides, it is found that after hydrothermal treatment for 4 h at 850 °C, the aging sample Cu@ZSM-5 still keep high NO_x reduction activity, as shown in Fig. 7e, suggestive of its excellent hydrothermal stability. More importantly, the crystal phase, the

distribution of Cu nanoclusters and chemical state of Cu species of the sample Cu@ZSM-5 after reaction is nearly unchanged (Figs. S6–8), confirming its super stability due to confinement effect.

To further explore the catalytic activity of these catalysts, the apparent activation energy (E_a) of NO_x conversion by steady-state kinetic measurements was also performed. It is known that the reduction of NO_x by NH_3-SCR is the first-order reaction. Based on the Arrhenius equation plots, the E_a of NO_x conversion of the samples Cu@ZSM-5, Cu/ZSM-5 and ZSM-5 are about 22.8, 32.3 and 37.1 kJ mol^{-1}, respectively (Fig. 7f). Obviously, Cu@ZSM-5 shows the lowest E_a among prepared catalysts, indicating that the reduction of NO_x by NH_3-SCR is more easily performed on the sample Cu@ZSM-5, which is consistent with the results of catalytic tests (Fig. 7a).

3.2. Catalytic tests on monolithic catalyst

Furthermore, the catalyst synthesis process is amplified and monolithic catalyst was prepared by coating catalyst slurry Cu@ZSM-5 inside of monolithic honeycomb channels, as shown in Fig. 8a. The NO_x and NH_3 conversion is shown in Fig. 8b-c. It is found that the conversion of NO_x is almost 100% at 200–450 °C, which can be attributed to fully exposed contact area. Meanwhile, the NH_3 oxidation is main side reaction, which can affect the NO_x conversion. The decline of NO_x conversion at high temperatures (> 450 °C) may be caused by NH_3 oxidation, which produces a large amount of NO_x and cannot fully react with insufficient NH_3 adsorbed, resulting in the decrease of NO_x conversion [42]. Additionally, the N_2O is by-products of NO_x reduction, and the decrease of N_2 selectivity at lower temperatures is mainly due to the production of N_2O from the non-selective reduction-oxidation reaction. Interestingly, the concentration of N_2O decreases significantly at higher temperature, probably because the strong acid sites of zeolite promote the deep reduction of NO_x. Notably, the N_2 selectivity can be kept at about 97% at 325–575 °C, suggestive of its high N_2 selectivity. The monolithic catalyst Cu@ZSM-5 without aluminum sol still shows super NO_x conversion, as shown in Fig. 8d, nevertheless, the conversion is slightly lower than that on the Cu@ZSM-5 with aluminum sol (Fig. 8b), since the addition of aluminum sol is conductive to increase the adhesion of catalyst slurry and improve the coating quality of catalyst. Notably, the NH_3 conversion on monolithic catalyst Cu@ZSM-5 with aluminum sol is extremely high at the beginning of the reaction but decreases at 250–300 °C (Fig. 8b), while the NH_3 conversion on monolithic catalyst Cu@ZSM-5 without aluminum sol increases gradually with increasing temperature (Fig. 8d), which can be explained that the addition of acidic aluminum sol is beneficial for the adsorption of NH_3 under lower temperature, while the adsorbed NH_3 will gradually desorb with the increasing temperature.

3.3. Catalytic mechanism

Fig. 9 shows *in-situ* FTIR spectra of surface adsorbed species over the sample Cu@ZSM-5 from the co-adsorption of NO, NH_3 and O_2 at different reaction condition. In the presence of NO, the bands at 3346, 3270 and 1065 cm^{-1} are related to the adsorption of NH_3 on the Cu active species. Meanwhile, the band at 1207 cm^{-1} is attributed to NH_3 bound to Lewis acid sites and the band at 1427 cm^{-1} is assigned to ionic NH_4^+ bound to Brønsted acid sites [43]. Besides, bidentate nitrate (1354 cm^{-1}) and the adsorbed NO_2 (1624 cm^{-1}) can be detected [44]. At 300 °C, with the increase of exposure time, the bands strength at 3346, 3270, 1065, 1624 and 1427 cm^{-1} weakens significantly, indicating that NH_4^+ bound to the Cu species and Brønsted acid site (1427 cm^{-1}) can react with NO_2. These results show that the Brønsted acid site of Cu@ZSM-5 plays an important role in the NH_3-SCR reaction at high temperature, which is consistent with the result of Fig. 7a.

The variation trend of *in-situ* FTIR spectra of the sample Cu@ZSM-5 in the presence of H_2O is similar to that in the absence of H_2O, as shown in Fig. 9b. The above results suggest that the catalyst has excellent water-resistance, and the adsorbed NH_3 on the catalyst can effectively react with NO_x species in the presence of H_2O. Further, *in-situ* FTIR spectra of the sample Cu@ZSM-5 have been investigated at different temperatures, as shown in Fig. 9c. From 100 °C to 200 °C, the band at 3254 cm^{-1} (NH_3 adsorbed Cu species) diminishes while the band at 1624 cm^{-1} (NO_2 species) and the band at 1321 cm^{-1} (bidentate nitrate) strengthen. It can be concluded that NO is firstly oxidized into NO_2, and the formed NO_2 can react with NH_3 adsorbed on Cu active sites at low temperatures. Therefore, Cu species is main active sites during NH_3-SCR of NO_x at lower temperatures, which is consistent with the result of Fig. 7a-b. From 200 °C to 400 °C, the intensity of the bands at 3346, 3254, 1624 and 1427 cm^{-1} gradually weaken with the increasing temperature, especially, the band intensity at 1427 cm^{-1} (NH_4^+ bound to the strong Brønsted acid site) significantly decrease. It indicates that the NH_3 adsorbed on both Cu active sites and strong Brønsted acid sites can react with NO_2, and the NH_3-SCR of NO_x can be greatly promoted due to the combined action of Cu species and strong Brønsted acid site, which is also identical to the test results of powder catalyst (Fig. 7a-b).

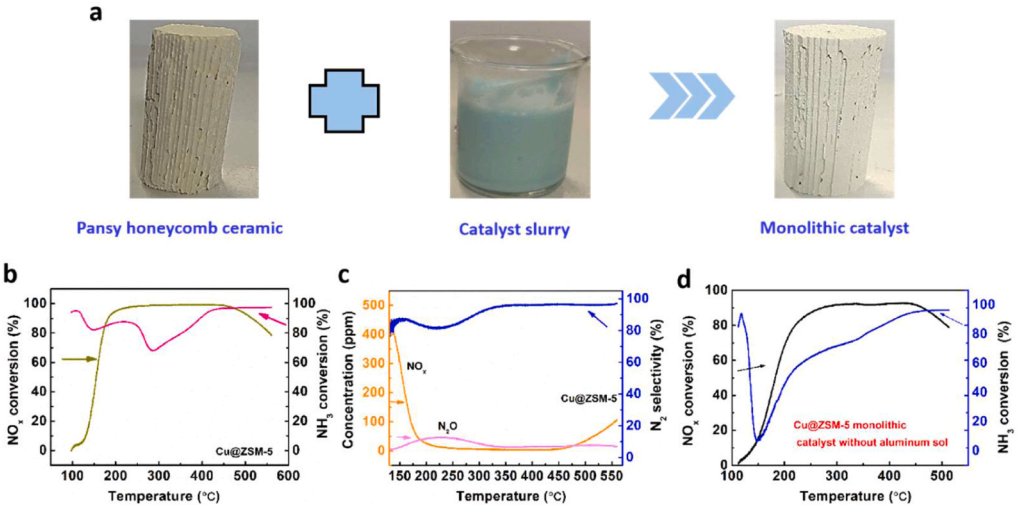

Fig. 8. a) The synthesis schematic diagram of monolithic catalyst Cu@ZSM-5 (2.4 mm × 2.4 mm×7.5 mm, catalyst content: 4.2 g), b) NO_x and NH_3 conversion of the monolithic catalyst Cu@ZSM-5 with aluminum sol, c) the concentration of NO_x and N_2O, and the N_2 selectivity. d) NO_x and NH_3 conversion of the monolithic catalyst Cu@ZSM-5 without aluminum sol. Reaction conditions: [NO_x] = 500 ppm, [NH_3] = 600 ppm, [O_2] = 8 vol%, [H_2O] = 8 vol%, N_2 balanced, and GHSV = 40000 h^{-1}.

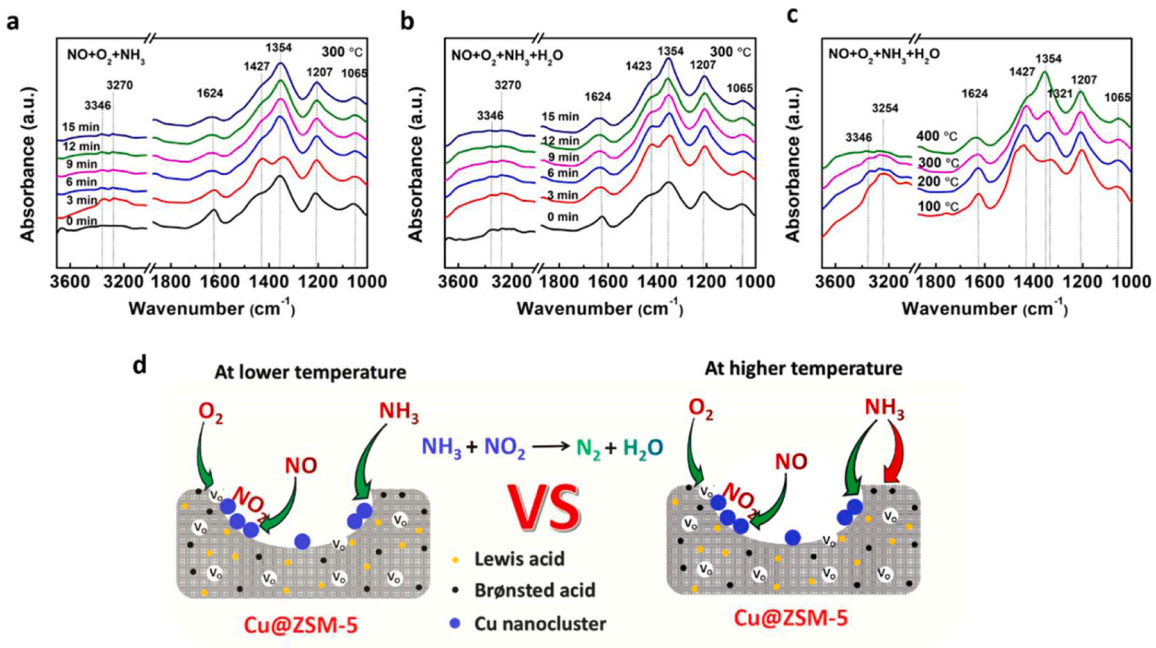

Fig. 9. In situ DRIFT spectra of the sample Cu@ZSM-5 at a) 300 °C in the presence of NH_3, NO and O_2, b) 300 °C and c) different temperatures in the presence of NH_3, NO, H_2O and O_2. d) The possible NH_3-SCR of NO_x mechanism on the sample Cu@ZSM-5. Reaction conditions: [NO_x] = 500 ppm, [NH_3] = 600 ppm, [O_2] = 8 vol%, [H_2O] = 8 vol%, N_2 balanced.

Based on the above results, a possible NH_3-SCR of NO_x mechanism on the sample Cu@ZSM-5 is proposed (Fig. 9d). Firstly, there are a larger number of oxygen vacancies presented in the sample Cu@ZSM-5 (Fig. 5d), accelerating the adsorption and activation of O_2. Meanwhile, a larger number of NO adsorbed on active sites can be firstly oxidized into NO_2, corroborated by *in-situ* FTIR (Fig. 9a-c). At lower temperature, the NH_3 adsorbed on Cu sites can react with NO_2 (Fig. 9c) and Cu species is the main active sites. Therefore, pure zeolite ZSM-5 has poor activity while Cu@ZSM-5 shows excellent activity at lower temperature (Fig. 7a). At higher temperature, the NH_3 adsorbed on both strong Brønsted acid sites of zeolite and Cu species, can react with NO_2 (Fig. 9b-c). Therefore, pure zeolite ZSM-5 has better catalytic activity at higher temperatures due to the existence of strong Brønsted acid sites. The catalytic activity of the sample Cu@ZSM-5 is significantly improved (Fig. 7a), which is ascribed to the combined effects of confined Cu nanoclusters and strong Brønsted acid sites.

4. Conclusions

A novel ZSM-5 zeolite-confined Cu nanoclusters catalyst Cu@ZSM-5 has been reported *via in-situ* self-assembly process. The resulting zeolite-confined catalyst Cu@ZSM-5 with higher concentration of Cu^+ shows remarkable NH_3-SCR of NO_x performance at wide temperature window, *i.e.*, the powder catalyst shows 98% NO_x conversion at 275–425 °C and the NO_x conversion is also above 90% at 225–550 °C, besides, it possesses the lowest activation energy and much better resistance to H_2O, which is superior than Cu/ZSM-5 sample prepared by the wet-impregnation method. Significantly, it shows remarkable performance and chemical stability with unchanged phase and chemical state after reaction. Interestingly, the conversion of NO_x on the monolithic catalyst Cu@ZSM-5 is almost 100% at 200–475 °C and the N_2 selectivity can be maintained at about 97% at 325–575 ℃. *In-situ* DRIFT tests proves that the strong Brønsted acid sites and Cu nanoclusters play a more critical role at higher temperature while Cu nanoclusters are main active sites at lower temperature during NH_3-SCR of NO_x. The highly dispersed and stable Cu nanoclusters confined into the mesoporous zeolite ZSM-5 benefit the adsorption and activation of reactants, greatly improving catalytic activity, water resistance and stability.

CRediT authorship contribution statement

Li Zhanyu: Methodology, Writing – original draft. **Sun Yuanyuan:** Conceptualization, Data curation, Methodology, Software. **Zhou Xiaoxia:** Funding acquisition, Writing – review & editing. **Chen Hangrong:** Validation, Writing – review & editing. **Tan Min:** Investigation. **Li Guohui:** Data curation. **Sun Wei:** Supervision. **Ao Shuang:** Software.

Declaration of Competing Interest

The authors declare that they have no known competing financial interests or personal relationships that could have appeared to influence the work reported in this paper.

Data Availability

Data will be made available on request.

Acknowledgements

This research was sponsored by National Natural Science Foundation of China (52272099), Key Research and Development Project of Ningxia (2022BFE03001), the Education Department of Hainan Province [Hnky2023–58], the Specific Research fund of Innovation Platform for Academicians of Hainan Province, Research Project of Qiongtai Normal University [qtqn202213], Provincial College Students Innovation and Entrepreneurship Training Program of Hainan Normal University [S202311658026/S202311658027].

Appendix A. Supporting information

Supplementary data associated with this article can be found in the online version at doi:10.1016/j.apcatb.2024.123747.

References

[1] L. Han, S. Cai, M. Gao, J.-y Hasegawa, P. Wang, J. Zhang, L. Shi, D. Zhang, Selective catalytic reduction of NO_x with NH_3 by using novel catalysts: state of the art and future prospects, Chem. Rev. 119 (2019) 10916–10976.

[2] A.G. Greenaway, A. Marberger, A. Thetford, I. Lezcano-Gonzalez, M. Agote-Aran, M. Nachtegaal, D. Ferri, O. Kroecher, C.R.A. Catlow, A.M. Beale, Detection of key transient Cu intermediates in SSZ-13 during NH_3-SCR deNO_x by modulation excitation IR spectroscopy, Chem. Sci. 11 (2020) 447–455.

[3] M. Chen, J. Li, W. Xue, S. Wang, J. Han, Y. Wei, D. Mei, Y. Li, J. Yu, Unveiling Secondary-Ion-Promoted Catalytic Properties of Cu-SSZ-13 Zeolites for Selective Catalytic Reduction of NO_x, J. Am. Chem. Soc. 144 (2022) 12816–12824.

[4] X. Huang, F. Dong, G. Zhang, Z. Tang, Design and identify the confinement effect of active site position on catalytic performance for selective catalytic reduction of NO with NH_3 at low temperature, J. Catal. 420 (2023) 134–150.

[5] X. Wu, H. Meng, Y. Du, J. Liu, B. Hou, X. Xie, Insight into Cu_2O/CuO collaboration in the selective catalytic reduction of NO with NH_3: Enhanced activity and synergistic mechanism, J. Catal. 384 (2020) 72–87.

[6] X. Wang, Y. Xu, M. Qin, Z. Zhao, X. Fan, Q. Li, Insight into the effects of Cu^{2+} ions and CuO species in Cu-SSZ-13 catalysts for selective catalytic reduction of NO by NH_3, J. Colloid Interface Sci. 622 (2022) 1–10.

[7] K.A. Tarach, M. Jabłońska, K. Pyra, M. Liebau, B. Reiprich, R. Gläser, K. Góra-Marek, Effect of zeolite topology on NH_3-SCR activity and stability of Cu-exchanged zeolites, Appl. Catal. B: Environ. 284 (2021) 119752.

[8] J. Du, S. Han, C. Huang, Y. Shan, Y. Zhang, W. Shan, H. He, Comparison of precursors for the synthesis of Cu-SSZ-39 zeolite catalysts for NH_3-SCR reaction, Appl. Catal. B: Environ. 338 (2023) 123072.

[9] H. Peng, T. Dong, S. Yang, H. Chen, Z. Yang, W. Liu, C. He, P. Wu, J. Tian, Y. Peng, X. Chu, D. Wu, T. An, Y. Wang, S. Dai, Intra-crystalline mesoporous zeolite encapsulation-derived thermally robust metal nanocatalyst in deep oxidation of light alkanes, Nature, Communications 13 (2022) 295.

[10] K. Guo, J. Ji, R. Osuga, Y. Zhu, J. Sun, C. Tang, J.N. Kondo, L. Dong, Construction of Fe_2O_3 loaded and mesopore confined thin-layer titania catalyst for efficient NH_3-SCR of NO_x with enhanced H_2O/SO_2 tolerance, Appl. Catal. B: Environ. 287 (2021) 119982.

[11] I. Song, H. Lee, S.W. Jeon, D.H. Kim, Controlling Catalytic Selectivity Mediated by Stabilization of Reactive Intermediates in Small-Pore Environments: A Study of Mn/TiO_2 in the NH_3-SCR Reaction, Acs Catal. 10 (2020) 12017–12030.

[12] R. Yan, S. Lin, Y. Li, W. Liu, Y. Mi, C. Tang, L. Wang, P. Wu, H. Peng, Novel shielding and synergy effects of Mn-Ce oxides confined in mesoporous zeolite for low temperature selective catalytic reduction of NO_x with enhanced SO_2/H_2O tolerance, J. Hazard. Mater. 396 (2020) 122592.

[13] D. Chen, A. Khetan, H. Lei, V. Rizzotto, J.-Y. Yang, J. Jiang, Q. Sun, B. Peng, P. Chen, R. Palkovits, D. Ye, U. Simon, Copper Site Motion Promotes Catalytic NO_x Reduction under Zeolite Confinement, Environ. Sci. Technol. 57 (2023) 16121–16130.

[14] H. Lei, D. Chen, J.-y Yang, A. Khetan, J. Jiang, B. Peng, U. Simon, D. Ye, P. Chen, Revealing the formation and reactivity of cage-confined Cu pairs in catalytic NO_x reduction over Cu-SSZ-13 zeolites by In Situ UV-Vis spectroscopy and time-dependent DFT calculation, Environ. Sci. Technol. 57 (2023) 12465–12475.

[15] Y. Wang, X. Ji, H. Meng, L. Qu, X. Wu, Fabrication of high-silica Cu/ZSM-5 with confinement encapsulated Cu-based active species for NH_3-SCR, Catal. Commun. 138 (2020) 105969.

[16] M. Hartmann, M. Thommes, W. Schwieger, Hierarchically-ordered zeolites: a critical assessment, Adv. Mater. Interfaces 8 (2021) 2001841.

[17] S. Thangudu, C.H. Wu, C.H. Lee, K.C. Hwang, Enhanced photofixation of dinitrogen to ammonia over a biomimetic metal (Fe,Mo)-doped mesoporous MCM-41 zeolite catalyst under ambient conditions, ACS Sustain. Chem. Eng. 9 (2021) 8748–8758.

[18] Z. Wang, R. Zhang, J. Wang, Z. Yu, Y. Xiang, L. Kong, H. Liu, A. Ma, Hierarchical zeolites obtained by alkaline treatment for enhanced n-pentane catalytic cracking, Fuel 313 (2022) 122669.

[19] S. Das, J. Ashok, Z. Bian, N. Dewangan, M.H. Wai, Y. Du, A. Borgna, K. Hidajat, S. Kawi, Silica-Ceria sandwiched Ni core-shell catalyst for low temperature dry reforming of biogas: Coke resistance and mechanistic insights, Appl. Catal. B: Environ. 230 (2018) 220–236.

[20] Z. Li, L. Mo, Y. Kathiraser, S. Kawi, Yolk-satellite-shell structured Ni-Yolk@Ni@SiO_2 nanocomposite: superb catalyst toward methane CO2 reforming reaction, ACS Catal. 4 (2014) 1526–1536.

[21] S.H. Joo, J.Y. Park, C.-K. Tsung, Y. Yamada, P. Yang, G.A. Somorjai, Thermally stable Pt/mesoporous silica core–shell nanocatalysts for high-temperature reactions, Nat. Mater. 8 (2009) 126–131.

[22] B. Liu, K. Zheng, Z. Liao, P. Chen, D. Chen, Y. Wu, Q. Xia, H. Xi, J. Dong, Fe-Encapsulated ZSM-5 Zeolite with Nanosheet-Assembled Structure for the Selective Catalytic Reduction of NO_x with NH_3, Ind. Eng. Chem. Res. 59 (2020) 8592–8600.

[23] C. Peng, R. Yan, H. Peng, Y. Mi, J. Liang, W. Liu, X. Wang, G. Song, P. Wu, F. Liu, One-pot synthesis of layered mesoporous ZSM-5 plus Cu ion-exchange: Enhanced NH_3-SCR performance on Cu-ZSM-5 with hierarchical pore structures, J. Hazard. Mater. 385 (2020) 121593.

[24] A.M. Garcia-Minguillan, L. Briones, M. Alonso-Doncel, J. Cejka, D.P. Serrano, J. A. Botas, J.M. Escola, One-pot synthesis of cyclohexylphenol via isopropyl alcohol-assisted phenol conversion using the tandem system RANEY (R) Nickel plus hierarchical Beta zeolite, Green. Chem. 24 (2022) 9168–9179.

[25] J. Zhao, L. Dong, Y. Wang, J. Zhang, R. Zhu, C. Li, M. Hong, Amino-acid modulated hierarchical In/H-Beta zeolites for selective catalytic reduction of NO with CH_4 in the presence of H_2O and SO_2, Nanoscale 14 (2022) 5915–5928.

[26] X. Zhou, Y. Chen, T. Ge, Z. Hua, H. Chen, J. Shi, Sodium carbonate-assisted synthesis of hierarchically porous single-crystalline nanosized zeolites, Sci. Bull. 62 (2017) 1018–1024.

[27] J. Luo, F. Gao, K. Kamasamudram, N. Currier, C.H.F. Peden, A. Yezerets, New insights into Cu/SSZ-13 SCR catalyst acidity. Part I: Nature of acidic sites probed by NH_3 titration, J. Catal. 348 (2017) 291–299.

[28] L. Wang, W. Li, S.J. Schmieg, D. Weng, Role of Brønsted acidity in NH_3 selective catalytic reduction reaction on Cu/SAPO-34 catalysts, J. Catal. 324 (2015) 98–106.

[29] Y. Chai, W. Dai, G. Wu, N. Guan, L. Li, Confinement in a Zeolite and Zeolite Catalysis, Acc. Chem. Res. 54 (2021) 2894–2904.

[30] Q. Zhao, C. Liao, G. Chen, R. Liu, Z. Wang, A. Xu, S. Ji, K. Shih, L. Zhu, T. Duan, In situ confined synthesis of a copper-encapsulated silicalite-1 zeolite for highly efficient iodine capture, Inorg. Chem. 61 (2022) 20133–20143.

[31] L. Yang, Q. Liu, R. Han, K. Fu, Y. Su, Y. Zheng, X. Wu, C. Song, N. Ji, X. Lu, D. Ma, Confinement and synergy effect of bimetallic Pt-Mn nanoparticles encapsulated in ZSM-5 zeolite with superior performance for acetone catalytic oxidation, Appl. Catal. B-Environ. 309 (2022) 121224.

[32] J. Hun Kwak, H. Zhu, J.H. Lee, C.H.F. Peden, J. Szanyi, Two different cationic positions in Cu-SSZ-13? Chem. Commun. 48 (2012) 4758–4760.

[33] R. Yu, H. Kong, Z. Zhao, C. Shi, X. Meng, F.-S. Xiao, T. De Baerdemaeker, A.-N. Parvulescu, U. Müller, W. Zhang, Rare-earth yttrium exchanged Cu-SSZ-39 zeolite with superior hydrothermal stability and SO_2-tolerance in NH_3-SCR of NO_x, ChemCatChem 14 (2022) e202200228.

[34] K. Chen, X. Wu, J. Zhao, H. Zhao, A. Li, Q. Zhang, T. Xia, P. Liu, B. Meng, W. Song, X. Zhu, H. Liu, X. Gao, C. Xu, B. Shen, Organic-free modulation of the framework Al distribution in ZSM-5 zeolite by magnesium participated synthesis and its impact on the catalytic cracking reaction of alkanes, J. Catal. 413 (2022) 735–750.

[35] N. Kalantari, M.F. Bekheet, P.D.K. Nezhad, J.O. Back, A. Farzi, S. Penner, N. Delibas, S. Schwarz, J. Bernardi, D. Salari, A. Niaei, Effect of chromium and boron incorporation methods on structural and catalytic properties of hierarchical ZSM-5 in the methanol-to-propylene process, J. Ind. Eng. Chem. 111 (2022) 168–182.

[36] H.Y. Chen, L. Chen, J. Lin, K.L. Tan, J. Li, Copper sites in copper-exchanged ZSM-5 for CO activation and methanol synthesis: XPS and FTIR studies, Inorg. Chem. 36 (1997) 1417–1423.

[37] J. Lei, R. Niu, S. Wang, J. Li, The Pd/Na-ZSM-5 catalysts with different Si/Al ratios on low concentration methane oxidation, Solid State Sci. 101 (2020) 106097.

[38] J. Guo, C. Guo, L. Chen, X. Peng, Modified mesoporous Y zeolite catalyzed nitration of azobenzene using NO_2 as the nitro source combined with density functional theory studies, N. J. Chem. 45 (2021) 21389–21394.

[39] R. Xu, Z. Wang, N. Liu, C. Dai, J. Zhang, B. Chen, Understanding Zn functions on hydrothermal stability in a one-pot-synthesized Cu&Zn-SSZ-13 catalyst for NH_3 selective catalytic reduction, ACS Catal. 10 (2020) 6197–6212.

[40] X. Su, Z. Jiang, J. Zhou, H. Liu, D. Zhou, H. Shang, X. Ni, Z. Peng, F. Yang, W. Chen, Z. Qi, D. Wang, Y. Wang, Complementary operando spectroscopy identification of in-situ generated metastable charge-asymmetry Cu_2-CuN_3 clusters for CO_2 reduction to ethanol, Nat. Commun. 13 (2022) 1322.

[41] R. Khairova, S. Komaty, A. Dikhtiarenko, J.L. Cerrillo, S.K. Veeranmaril, S. Telalović, A.A. Tapia, J.-L. Hazemann, J. Ruiz-Martinez, J. Gascon, Zeolite synthesis in the presence of metallosiloxanes for the quantitative encapsulation of metal species for the selective catalytic reduction (SCR) of NO_x, Angew. Chem. Int. Ed. 62 (2023) e202311048.

[42] T. Yu, T. Hao, D. Fan, J. Wang, M. Shen, W. Li, Recent NH_3-SCR mechanism research over Cu/SAPO-34 Catalyst, J. Phys. Chem. C. 118 (2014) 6565–6575.

[43] J. Liu, X. Li, Q. Zhao, J. Ke, H. Xiao, X. Lv, S. Liu, M. Tadé, S. Wang, Mechanistic investigation of the enhanced NH_3-SCR on cobalt-decorated Ce-Ti mixed oxide: In situ FTIR analysis for structure-activity correlation, Appl. Catal. B: Environ. 200 (2017) 297–308.

[44] L. Chen, R. Li, Z. Li, F. Yuan, X. Niu, Y. Zhu, Effect of Ni doping in $Ni_xMn_{1-x}Ti_{10}$ (x = 0.1-0.5) on activity and SO_2 resistance for NH_3-SCR of NO studied with in situ DRIFTS, Catal. Sci. Technol. 7 (2017) 3243–3257.